Check for updates

Received: 30 June 2020 | Revised: 28 October 2020 | Accepted: 18 December 2020

DOI: 10.1111/jace.17682

Journal of the American Ceramic Society

ORIGINAL ARTICLE

Sintering-driven effects on the band gap of (Pb,La)(Ti,Ni)O_3 photovoltaic ceramics

Natália F. C. Vargas[1] | **Mahmoud S. Alkathy**[2] | **José A. Eiras**[2] | **Valmor Roberto Mastelaro**[3] | **Manuel H. Lente**[1]

[1]Instituto de Ciência e Tecnologia, Universidade Federal de São Paulo, Sao Paulo, Brazil

[2]Departamento de Física, Universidade Federal de São Carlos, São Carlos, Brazil

[3]Instituto de Física de São Carlos, Universidade de São Paulo, São Carlos, Brazil

Correspondence
Manuel H. Lente, Instituto de Ciência e Tecnologia, Universidade Federal de São Paulo, São José dos Campos, Sao Paulo, SP CEP 12231-280, Brazil.
Email: mlente@unifesp.br

Funding information
Conselho Nacional de Desenvolvimento Científico e Tecnológico; Financiadora de Estudos e Projetos; Fundação de Amparo à Pesquisa do Estado de São Paulo, Grant/Award Number: 2017/13769-1 and 2019/03110-8

Abstract

In this work, the influence of the sintering temperature on the physical properties of $(Pb_{0.8}La_{0.2})(Ti_{0.9}Ni_{0.1})O_3$ (PLT-Ni) ceramics is reported. The experimental data revealed that the energy band gap of PLT-Ni ceramics could be tailored from approximately 2.7 to 2.0 eV by changing the sintering temperature from 1100°C to 1250°C. It is demonstrated that the simple substitution of Ti^{4+} by Ni^{2+} cations is effective to decrease the intrinsic band gap while increasing the tetragonality factor and the spontaneous polarization. However, the additional red-shift observed in the absorption edge of the PLT-Ni with increasing the sintering temperature was associated with a continuous increase in the oxygen vacancies (V_O^{2-}) amount. It is believed that the impact of the creation of these thermally induced V_O^{2-} is manifold. The presence of V_O^{2-} and Ni^{2+} ions generate the Ni^{2+}-V_O^{2-} defect-pairs that promoted both a decrease in the intrinsic band gap and an additional increase of the tetragonality factor, consequently, increasing the spontaneous polarization. The creation of Ni^{2+}-V_O^{2-} defects also changed the local symmetry of Ni^{2+} ions from octahedral to a square pyramid, thus lifting the degeneracy of the Ni^{2+} 3*d* orbitals. With the increase in the sintering temperature, lower-energy absorbing intraband states were also formed due to an excess of V_O^{2-}, being responsible for an add-on shoulder in the absorption edge, extending the light absorption curve to longer wavelengths and leading to an additional absorption in "all investigated" spectrum as well.

KEYWORDS

dielectric materials/properties, electroceramics, ferroelectricity/ferroelectric materials, photovoltaic, sinter/sintering

1 | INTRODUCTION

ABO_3 ferroelectric oxides are promising candidates for light-absorbing materials for applications in solar-energy conversion devices.[1-5] Nevertheless, they present a wide intrinsic band gap (3–5 eV), absorbing light only in the UV region, resulting in a small efficiency.[6] Then, it is imperative to narrow their band gap for technological viability. Furthermore, in conventional solar cells, the p-n junctions create a built-in electric field that separates the photoelectrons and holes. In the case of ferroelectrics, the strategy is that the ferroelectric polarization induces an intrinsic built-in field, thus contributing to the photoinduced charge carrier's separation.[7] Then, it is also desirable to maintain a ferroelectric polarization, while narrowing the band gap. In this context, it has been proposed that by a suitable band gap-engineering the intrinsic band gap of ferroelectric oxides can be decreased, maintaining the polarization.[6,8-10]

Aliovalent transition-metal cations (M^{n+}) are thus introduced into the *B*-site, being stabilized by the formation of oxygen vacancies (V_O^{2-}).

Among possible ferroelectric oxides that may be employed as visible light-absorbing materials, lead titanate ($PbTiO_3$) is the prototype candidate.[6,8] It presents a high tetragonality factor ($c/a \approx 1.063$) and a sharp peak in dielectric permittivity at the Curie temperature.[11] In $PbTiO_3$, the highest occupied molecular orbital (HOMO) is localized around the O atom. Its 2*p* orbitals interact/overlap slightly with the 3*d* of Ti^{4+} and the 6*s* orbitals of Pb 6, while the lowest unoccupied molecular orbital (LUMO) lies around the Ti^{4+} and resembles 3*d* states.

It was proposed that by substituting the *B*-site of $PbTiO_3$ with Ni^{2+}, stabilized by an accompanying V_O^{2-}, the intrinsic band gap may be lowered.6 Moreover, it was predicted that the introduction of Ni^{2+}-V_O^{2-} defect-pairs increases all cation displacements and, thus, increasing the spontaneous polarization.6 In comparison to undoped $PbTiO_3$, the band gap narrowing is induced by the presence of Ni^{2+} in the electronic structure of both the HOMO and LUMO.6 The band gap tailoring in $Pb(Ti,Ni)O_{3-\delta}$ was theoretically investigated introducing only Ni^{2+} ions substituting Ti^{4+} and creating the exact amount of V_O^{2-} to form Ni^{2+}-V_O^{2-} defect-pairs to reach the electronic neutrality of the lattice.[6,12] A discussion about the influence of V_O^{2-} unbalance on the band gap of $Pb(Ti,Ni)O_{3-\delta}$ is still missing.

To promote a nominally charge-balancing in $Pb(Ti,Ni)O_{3-\delta}$, an alternative is to introduce into the *A*-site ions with valence higher than the Pb^{2+}, such as La^{3+}. By suitable La^{3+} co-doping, the formation of V_O^{2-} could be theoretically inhibited, allowing, in principle, the investigation of the direct contribution of the Ni^{2+} ions in the band gap narrowing. However, from the ceramic processing point of view, oxygen vacancies can be still formed, due to the need of high sintering temperatures under long dwell times[13,14] and due to their relative low formation energy.[15]

In this context, it was shown that by introducing V_O^{2-} into the crystal lattice of some metal oxides, the light absorption could be tuned from the UV to the visible range due to formation of localized defect states below the conduction band edge.[16-18] These defect states are responsible for an add-on shoulder in the absorption edge, extending the light absorption curve to longer wavelengths, which is often called Urbach tail.[19] The energy associated with the width of this tail is the Urbach energy.[20,21] In this case, there is no true narrowing of the intrinsic band gap, but instead only an introduction of energy levels within the forbidden band due to shallow- and/or deep-level states. Thus, the Urbach energy due to these defect states results only in an "apparent" intrinsic band gap narrowing. The ideal case occurs when doping narrows the intrinsic band gap.[22] Therefore, V_O^{2-} is one of the most important defects for the optical absorption properties.[23,24]

In this work, it is reported that the influence of the sintering temperature on the physical properties of nominally charge-compensated $(Pb_{0.8}La_{0.2})(Ti_{0.9}Ni_{0.1})O_3$ ceramics. The initial idea is to investigate separately the contribution of Ni^{2+} on the band gap narrowing in the $(Pb_{0.8}La_{0.2})(Ti_{0.9}Ni_{0.1})O_3$, avoiding, a priori, the formation of V_O^{2-} by La^{3+}co-doping. Nevertheless, the experimental data revealed that all investigated physical properties had been modified by changing the sintering temperature. The results are discussed in terms of the generation of unavoidable defects and/or changes in the crystal structure introduced during the sintering, probably, due to a gradual formation and or migration of oxygen vacancies in the O_6 octahedron.

2 | EXPERIMENTAL PROCEDURE

Nominally charge-balanced $(Pb_{0.8}La_{0.2})(Ti_{0.9}Ni_{0\cdot1})O_3$ (PLT-Ni) ceramics were prepared by the conventional mixed-oxide process. La^{3+} ions were introduced into the *A*-site to avoid the formation of oxygen vacancies due to the Ni^{2+} doping.

PbO (litharge), TiO_2 (anatase), La_2O_3, and NiO (from Sigma-Aldrich, >99.0% purity) were used as precursor materials. The precursor powders were mixed in a ball milling for 3.0 h by using ethanol and ZrO_2 balls. The mixed powders were calcined at 800°C for 3.5 h. The calcined powders were isostatically pressed under 250 MPa in disk shapes. The pressed green bodies were sintered under different sintering temperatures for a dwell time of 2.0 h at a heating rate of 5°C/min. All samples were sintered in an alumina closed crucible in a saturated PbO atmosphere. The sintered samples were polished to a thickness of ~1.0 mm. Scanning electron microscopy (SEM) (FEI Company, Inspect S50) was employed for microstructural evaluations. Gold electrodes were sputtered on the samples. The structures of the ceramic pellets were characterized at room temperature by X-ray diffraction (Ultima IV, Rigaku) using Cu-K_α radiation and by the Rietveld method. The bulk densities of the sintered samples were determined by the geometrical method. X-ray Photoelectron Spectroscopy (XPS) measurements of the sintered pellets were carried out in Scienta Omicron ESCA+spectrometer with monochromatic X-ray source Al-Kα (1486.7 eV, with a power of 280 W and a constant pass energy mode of 50 eV). The XPS high-resolution peaks were deconvoluted using a Pseudo-Voigt function after subtracting a Shirley background using CASA XPS software. The binding energies were measured about the C 1s peak at 284.8 eV.

Diffuse reflectance spectroscopy investigation was performed at room temperature by using a UV-VIS spectrophotometer (Shimadzu 2600) equipped with an integrating sphere. Dielectric characterizations were made using an HP 4194A in the heating of 2°C/min. Ferroelectric

hysteresis loops were measured at room temperature using a Sawyer Tower circuit with a 10 Hz sinusoidal wave. Thermal expansion measurements of the sintered pellets were performed using a NETZSCH 402 dilatometer. The measurements were done at the heating of 5°C/min in the atmosphere.

3 | RESULTS AND DISCUSSION

Figure 1A shows the XRD patterns of the PLT-Ni ceramics sintered at different temperatures. Pure perovskite phases are seen in all sintered ceramics under investigation and there is no trace of any secondary phases indicating that the Ni amount has been successively dissolved into the PLT lattice. Moreover, all the observed peaks are indexed in tetragonal crystals systems which matched with standard ICSD60188 of perovskite $PbTiO_3$ ceramics.[25] To investigate the effect of sintering temperature on the crystal structure of PLT-Ni ceramics, a fine XRD pattern of PLT-Ni sintered samples in the 2θ range of 44–47° are exhibited in Figure 1B. The XRD patterns in Figure 1A,B confirms that the PLT-Ni ceramics sintered at different temperatures show typically tetragonal crystal symmetry which can be proven by the splitting peaks of (002)/(200) and the presence of single (110) peak. Also, it is observed that the intensity of the (002) and (200) peaks tend to increase with increasing in sintering temperature. This fact suggests a rise in tetragonality factor (*c*/*a*) with increasing sintering temperature.

Figure 1B shows the sintering temperature dependence of the geometric density of the ceramic bodies. It is seen that the bulk density increases with increasing the sintering temperature from 1100 up to 1250°C. For samples sintered at 1262°C (not shown here) secondary phase was detected and at higher temperatures, the samples melt. Some authors have modeled and experimentally found that grain-boundary diffusion and interface reaction are the dominating mechanisms involved in the densification process of PZT ceramics.[26] Since the coarsening phenomenon was not observed in our samples (see discussions below), it is believed that such mechanisms were responsible for the densification process in the PLT-Ni system.

From the XRD data, analyzed through the Rietveld method, Figure 1B reveals that the tetragonality factor (*c*/*a* ratio) increases by increasing the sintering temperature. The maximum value reached for *c*/*a* was ≈1.0123, which is similar to that found for $(Pb_{0.8}La_{0.2})TiO_3$ ceramics.[27,28] To further prove the crystal structure and lattice parameters estimation and analysis with sintering temperatures of PLT-Ni, XRD Rietveld refinements supported by Fullprof software are presented in Supporting Information (Figure S4).

The insets in Figure 1B show the pictures of the as-sintered ceramic bodies as a function of the respective sintering temperature. The pictures reveal that the color of the samples changes from yellow-green, greenish pale color, green to finally become dark-green at higher temperatures. These pictures qualitatively reveal a remarkable influence of the sintering temperature on the optical proprieties. Changes

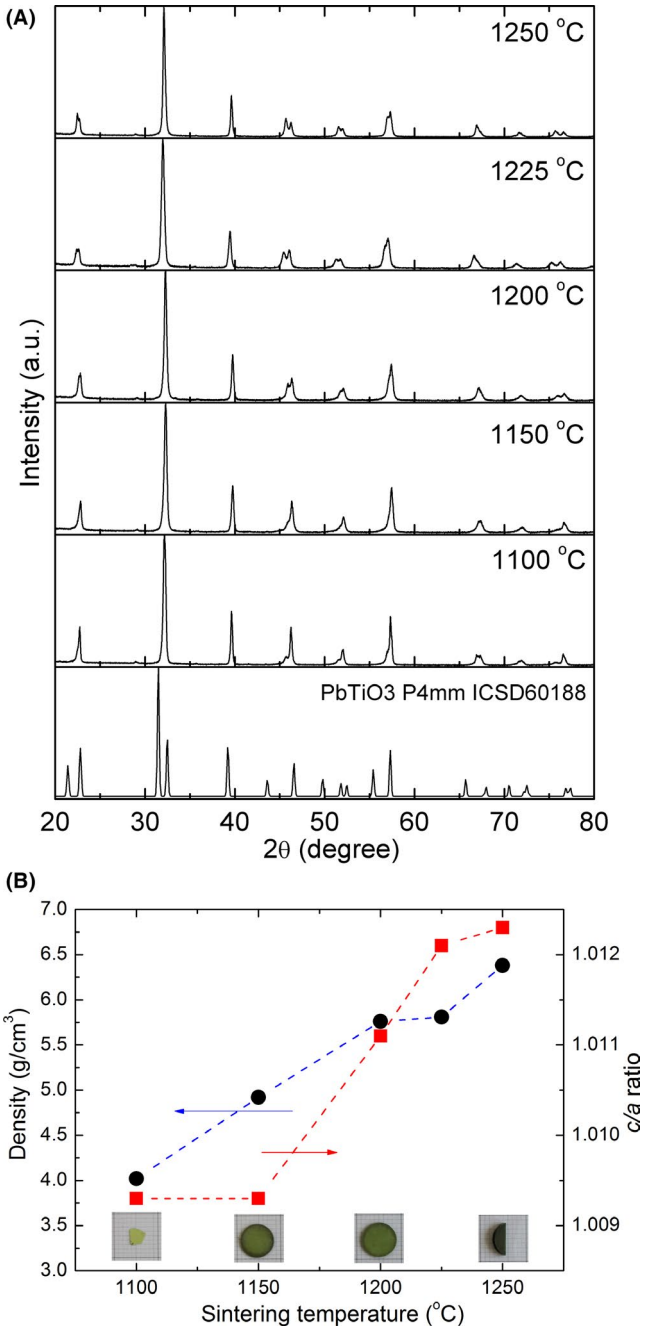

FIGURE 1 (A) XRD patterns of the $(Pb_{0.8}La_{0.2})(Ti_{0.9}Ni_{0.1})O_3$ ceramics sintered at different temperatures, and the right graph is the enlargement of the (002) and (200) peaks splitting. (B) Sintering temperature dependence of both the density and the *c*/*a* ratio of the ceramic bodies. Insets in B shows pictures of the as-sintered ceramic bodies, taken at room temperature, for the respective sintering temperatures [Color figure can be viewed at wileyonlinelibrary.com]

in the optical properties, as observed here (color of the samples), have only been noticed by increasing the doping amount in the parent $[KNbO_3]_{1-x}[BaNi_{1/2}Nb_{1/2}O_{3-\delta}]_x$ ferroelectric compositions.[1,2]

Figure S1a,b show the SEM images of the surface of the samples densified at 1100°C and 1250°C respectively. Both samples present a homogeneous microstructure. The sample sintered at low temperature (Figure S1a) reveals a smaller average grain size (~0.8 μm) than that densified at 1250°C (~2 μm).

Figure S2 shows the ferroelectric hysteresis loops for the samples sintered at 1100°C and 1250°C. The sample densified at 1250°C presents squarer hysteresis shape with higher polarization values than that sintered at 1100°C. This higher polarization is in agreement with the data from Figure 1B since higher *c*/*a* ratio results in higher polarization.[29] The inset in Figure S2 highlights that the hysteresis for the samples sintered at 1100°C reveals a rounded-shape curve, typical of conductivity due to incomplete densification.[30]

Figure 2A,B depict the temperature and frequency dependence of the dielectric permittivity of the PLT-Ni ceramics sintered at 1100°C and 1250°C, respectively. The sample sintered at higher temperatures presents higher values for ε′ and sharper peaks (around 150°C) on the dielectric curve than those observed for the sample sintered at 1100°C. These temperatures agree with those reported for the ferroelectric-paraelectric phase transition for "pure" PLT20.[27,28] The long-range ferroelectric order reflects in the sharp temperature dependence of the dielectric curve, while in relaxor-like ferroelectric the shorter-range order reflects in a broad dielectric curve. Comparing these results with Figure 1B, it is noticed that higher is the *c*/*a* ratio, sharper are the dielectric peaks and more displacive is the ferroelectric-paraelectric (FE-PE) phase transition.

The results of thermal strain and thermal strain rate measurements for the PLT-Ni ceramics are shown in Figure 3A,B, respectively. In Figure 3A, it is noticed that the sample sintered at the lowest temperature (1100°C) does not reveal a well-defined and abrupt/sharp minimum in the strain curve in the temperature region where the dielectric permittivity presents a peak. Indeed, the strain curve presents a broad maximum, a typical shape found for diffuse phase transition in relaxor-like ferroelectrics.[31,32] However, by increasing the sintering temperature, a more abrupt minimum in the strain curves is noticed. For the sample sintered at 1250°C a clear minimum in the strain curve is seen at around 160°C (Figure 3B), characteristic of a more displacive FE-PE phase-transition. Thus, in essence, the results in Figure 3 reveal that the nature of the ferroelectric phase transition for the PLT-Ni ceramics changes by increasing the sintering temperature. It is worth noting that sharper the dielectric peak curve (Figure 2), sharper is the thermal expansion rate curves (Figure 3).

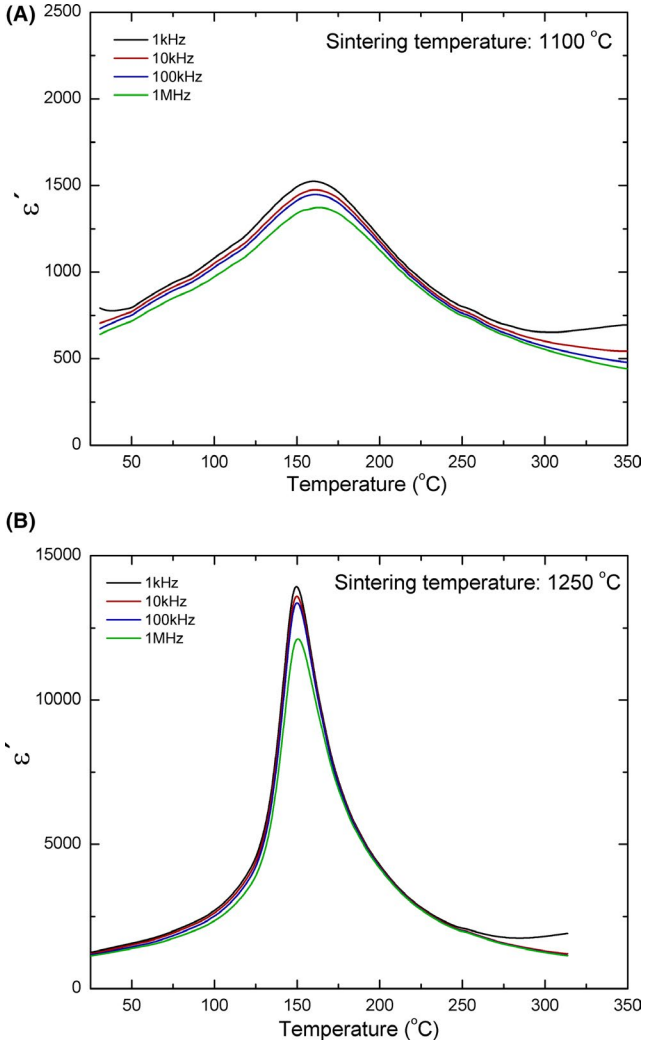

FIGURE 2 Temperature and frequency dependence of the real component of the dielectric permittivity of $(Pb_{0.8}La_{0.2})(Ti_{0.9}Ni_{0.1})O_3$ ceramics sintered at (A) 1100°C, and (B) 1250°C [Color figure can be viewed at wileyonlinelibrary.com]

Figure 4 shows the spectral dependence of the absorbance of the PLT-Ni ceramics. For the sake of comparison, the absorbance data for $PbTiO_3$ is also shown. The absorbance spectrum for the sample sintered at 1100°C presents a relatively sharp optical absorption edge around 550 nm. But by increasing the sintering temperature from 1100°C to 1250°C distinct behavior in the absorption spectra are gradually seen. First, intrinsic band gap energy presents an apparent redshift. Second, additional intra-band absorbing states, at lower energies, are created. These intra-band states would be responsible for the absorption increase in "all investigated" spectrum. Moreover, the absorption spectrum for the sample sintered at 1250°C exhibits a more remarkable add-on shoulder around 475 nm and a broader and diffused tail, which makes it impossible to determine precisely the band edge.[33] Although subtle, such add-on shoulder can be also noticed in the absorption curve of the sample sintered at 1225°C.

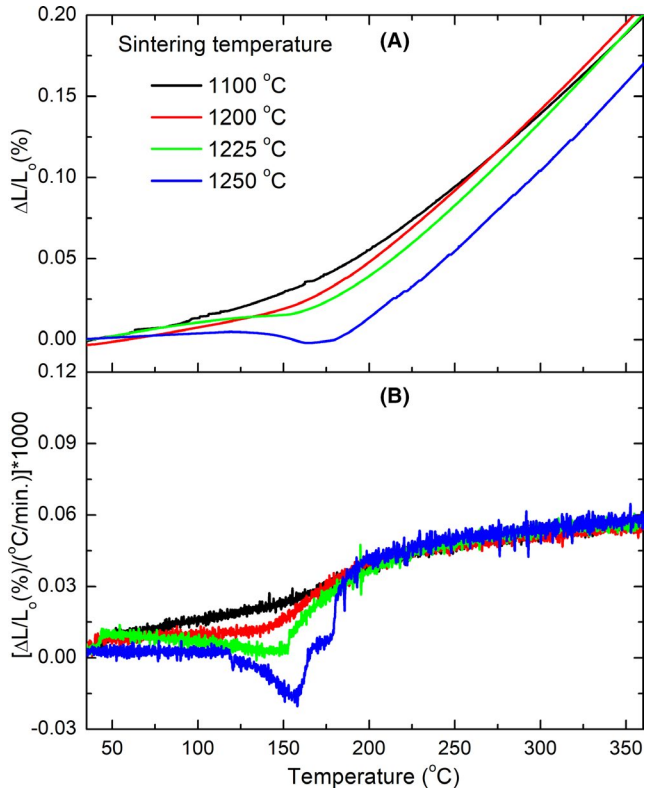

FIGURE 3 Thermal-strain measurements for the $(Pb_{0.8}La_{0.2})(Ti_{0.9}Ni_{0.1})O_3$ ceramics sintered at different temperatures. (A) thermal strain; (B) thermal strain rate [Color figure can be viewed at wileyonlinelibrary.com]

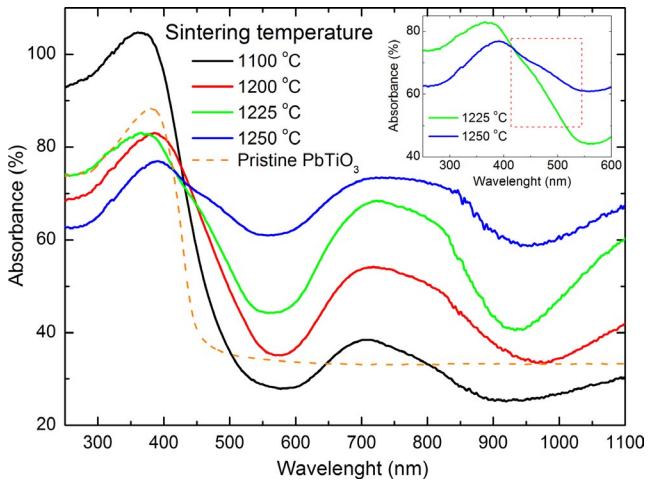

FIGURE 4 Spectral dependence of absorbance of the $(Pb_{0.8}La_{0.2})(Ti_{0.9}Ni_{0.1})O_3$ ceramics sintered at different temperatures. The absorbance spectrum for the pristine $PbTiO_3$ is also shown [Color figure can be viewed at wileyonlinelibrary.com]

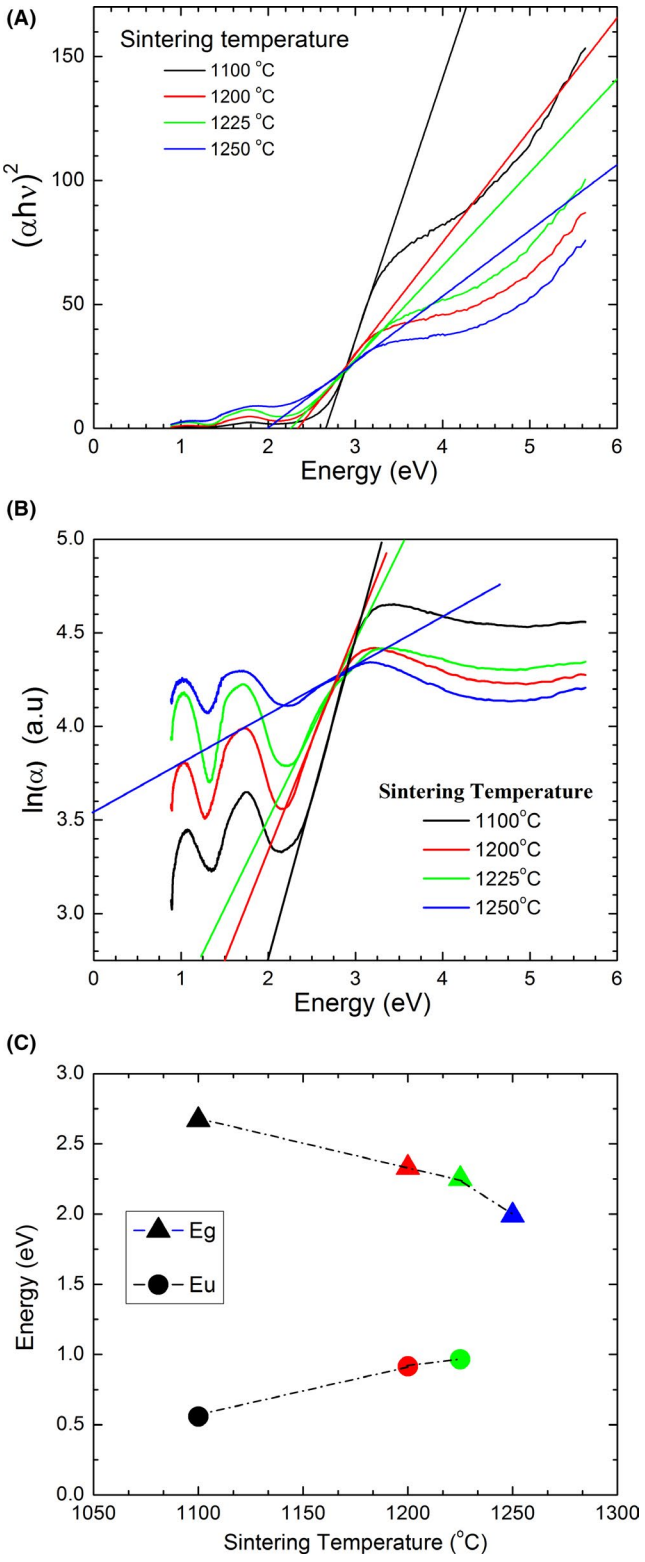

FIGURE 5 (A) Tauc plot, (B) Urbach plot and (C) the band gap energy for direct transition (E_g) and the Urbach energy (E_u) for the sintered pellets [Color figure can be viewed at wileyonlinelibrary.com]

Figure 5A–C show (A) the Tauc plot, (B) the Urbach plot and (C) the band gap energy for the direct transition (E_g) and the Urbach energy (E_u) for the sintered pellets. Figure 5C shows that E_g decreases from 2.67 eV to 1.99 eV, while E_u increases with increasing the sintering temperature. The increase in the Urbach energy is attributed to an increase in the concentration of oxygen vacancies, with energies at the boundaries of the energy gap, resulting in an apparent

band gap decreasing.[20,21] The E_u energy for the sample sintered at 1250°C (Figure 5B) resulted in a meaningless value (3.98 eV) and, thus, it was not inserted in Figure 5C.

Apart from the absorption edge, the spectral curves of the PLT-Ni present also some interesting features. In Figure 5A,B, it seems three peaks slightly dependent on the temperature that is located at around 1.75, 1.52 and 1.11 eV. As discussed in previous work,[34] and assuming a priori that such approach is valid for the PLT-Ni system, under strong enough perturbation, the degeneracies of the ${}^3T_{2g}(t_{2g}^5e_g^3)$, ${}^3T_{1g}(t_{2g}^5e_g^3)$ and ${}^3T_{1g}(t_{2g}^4e_g^4)$ triplet excited states of the Ni^{2+} can be lifted. Quickly, it was inferred that the peak located at around 1.75 eV could be associated with the superposition of ${}^1B_2[{}^1E_g(t_{2g}^6e_g^2)]$ ${}^1A_1[{}^1E_g(t_{2g}^6e_g^2)]$ and states. Also, the band near 1.52 eV would arise from the transitions ${}^3B_2^0 \rightarrow {}^3A_2[{}^3T_{1g}(t_{2g}^5e_g^3)]$, ${}^3B_2^0 \rightarrow {}^3B_2[{}^3T_{1g}(t_{2g}^5e_g^3)]$ and ${}^3B_2^0 \rightarrow {}^3B_1[{}^3T_{1g}(t_{2g}^5e_g^3)]$. Finally, the peak near 1.06 eV should correspond to the ${}^3A_{2g}(t_{2g}^6e_g^2) \rightarrow {}^3T_{2g}(t_{2g}^5e_g^3)$ transitions. For the PLT-Ni, the unit cell distortion (c/a) is always higher than 1 and it increases with increasing the sintering temperature. Since the local symmetry can allow the Ni *d-d* transitions in the host lattice, it could be inferred that the transitions describe above could be associated with the inherent lower symmetry on the PLT-Ni ceramics. Moreover, the gradual elongation of the octahedral cage (c/a ratio) would contribute to additional changes in the crystal field and, being responsible for the slight changes observed in the position of the peaks.

The results in Figures 1B, 4 and 5 show that is possible to tailor the optical absorption edge of $(Pb_{0.8}La_{0.2})(Ti_{0.9}Ni_{0.1})O_3$ ceramics by controlling the sintering temperature, still maintaining a macroscopic ferroelectric polarization. Similar behavior was also reported, but for a sample with a cubic structure on average.[34]

When compared to $PbTiO_3$, the data from the absorbance curves of $(Pb_{0.8}La_{0.2})(Ti_{0.9}Ni_{0.1})O_3$ revealed that, independently of the sintering temperature, the substitution of Ti^{4+} by Ni^{2+} decreased the band gap, as theoretically predicted for $Pb(Ti,Ni)O_{3-\delta}$[6,8] and observed in some works.[1,2,35-37] Although our composition is nominally charged neutral, our data show that the replacement of Ti^{4+} by Ni^{2+} is the main contribution to narrow the band gap, in comparison to the parent $PbTiO_3$.

From here, it prospects the possible mechanisms involved in the gradual changes of the absorption curve of $(Pb_{0.8}La_{0.2})(Ti_{0.9}Ni_{0.1})O_3$ activated by the sintering. It is stressed that the starting stoichiometry is the same for all nominally charge-balanced sintered pellets. However, it is necessary to take into account the introduction of unavoidable defects and/or defects rearrangement into the lattice during the sintering to interpret these results.

As mentioned earlier, the introduction of oxygen vacancies into the lattice may contribute to introduce sub-band defect states, which increase the absorption strength for lower energy radiation. These sub-band defect states lead to an apparent band gap narrowing, reflected in the appearance of an add-on shoulder on the edge of the absorption curve. Apparent intrinsic band gap narrowing exclusively due to the formation of V_O^{2-} in $LiNbO_3$ was already reported.[38] To describe the changes in the optical properties of PLT-Ni samples; it is considered in this work that by increasing the sintering temperature the relative amount of V_O^{2-} is increased due to oxygen volatilization and its ordering or redistribution in the lattice may also occur.[15]

To investigate the presence and evolution of V_O^{2-} and the role of the other ions in the PLT-Ni, their surface electronic structures were investigated by XPS. Figure 6A,B show the Ni 2*p* and O 1 *s* XPS high-resolution spectra for the PLT-Ni samples sintered at 1100°C and 1250°C respectively. The XPS spectra of the Ti 2*p*, La 3*d*, Pb 4*f* are shown in Figure S3a,b. The XPS spectrum of the Pb, Ti, La, and Ni elements are quite similar for both samples, whereas the spectrum of O 1*s* is significantly different.

Concerning the Ti 2*p* XPS spectrum, the first component, around 458 eV, is attributed to the Ti $2p_{3/2}$ peak, whereas the second one around 463 eV is ascribed to the Ti $2p_{1/2}$ peak. The energy positions of both peaks coincide well with previous reports on different ferroelectric perovskites compounds.[39,40] The difference between Ti $2p_{3/2}$ and Ti $2p_{1/2}$ spin-orbit splitting, which is around 5.5 eV, corresponds to Ti^{4+} oxidation state. As shown in Figure S3a,b, the Pb 4*f* XPS spectrum exhibits two components at approximately 137.9 and 142.8 eV, which are related to the Pb $4f_{7/2}$ and Pb $4f_{5/2}$ respectively. These peak positions correspond to Pb^{2+} presents in the material lattice.[40] It is seen in Figure S3a,b that the binding energies of La $3d_{5/2}$ are between 834.2 and 837.9 eV, confirming the existence of only La^{3+} ions.[41] The energy difference between these peaks is about 4 eV, also in good agreement with the literature.

The XPS La $3d_{3/2}$ spectrum overlaps with the Ni 2*p* XPS spectrum, making it difficult to quantitatively analyze the nickel XPS spectrum. However, qualitatively, the nickel spectrum for both samples are very similar, which would indicate that there is no change in the oxidation state of nickel caused by the differences in the sintering conditions. The La $3d_{3/2}$ and Ni 2*p* XPS spectra of both samples were deconvoluted in seven peaks corresponding to an overlapping of the La $3d_{3/2}$ and Ni $2p_{3/2}$ and Ni $2p_{1/2}$ levels.

As discussed before, the O 1*s* spectra of PLT-Ni samples are quite different for the samples sintered at 1100°C and 1250°C. The O 1*s* XPS spectra for both samples were deconvoluted in three peaks ranging from 529.0 to 532.2 eV. According to the literature,[42,43] the peak O 1*s* peak between 529.0 and 530.0 eV corresponds to the oxygen belonging to the sample network, while the O 1*s* peak located at approximately 531.0 eV was attributed

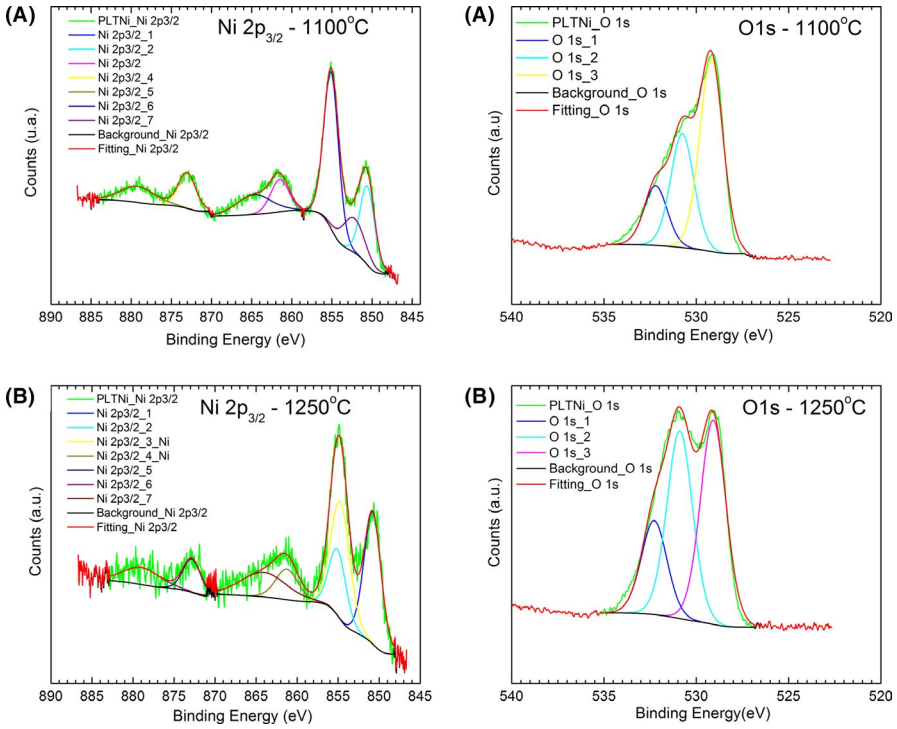

FIGURE 6 X-ray Photoelectron Spectroscopy spectra of $(Pb_{0.8}La_{0.2})(Ti_{0.9}Ni_{0.1})O_3$ ceramics sintered at (A) 1100°C, and (B) 1250°C [Color figure can be viewed at wileyonlinelibrary.com]

to oxygen vacancies. Therefore, the first peak located around 529.0 eV can be attributed to lattice oxygen in the PLT-Ni samples. According to XPS analysis, the amount of this oxygen specie is 52.8% for the sample sintered at 1100°C and 42.0% for the sample sintered at 1250°C, meaning that the lattice oxygen concentration decreased as the sintering temperature increased. The second peak situated around 530.8 eV is attributed to the existence of oxygen vacancies. In this case, our results show the presence of 31.0% and 42.0% of this specie for the 1100°C and 1250°C samples, respectively, indicating that the number of oxygen vacancies increased as the sintering temperature increased. The third peak, located around 532.2 eV, has been attributed to adsorbed oxygen, which amount was determined as equal to 16.2% and 19.3% for the 1100°C and 1250°C samples. In summary, the XPS results show a decrease in the amount of lattice oxygen (an increase of V_O^{2-}), in the samples as the sintering temperature increases.

The component of the lower binding energy (O1) is attributed to O^{2-} ions in the PLT structure and the component of higher binding energy (O2) are attributed to O^{2-} in oxygen-deficient regions in the PLT matrix. Moreover, this component (O2) is thought to be associated with the oxygen vacancy concentrations (VO), ie the variation in the O2/O1 ratio is related to changes in VO concentrating.[44] In our study, the O2/O1 ratio was found to be around 0.6 and 1.0 for the samples sintered at 1100°C and 1250°C respectively. The XPS result indicates that the concentration of oxygen vacancy increases with increase the sintering temperature and that reflects in the color change of the sintered pellets and the band gap decreasing with increases the absorption intensity in the visible region. Therefore, as inferred earlier, oxygen vacancies are the unavoidable defects introduced into the lattice during the sintering.

Following theoretical works,[6,8,12] the defect-pairs Ni^{2+}-O and Ni^{2+}-V_O^{2-} would be responsible for new HOMO and LUMO states and, thus by a true intrinsic band gap narrowing up to the saturation of the formation of Ni^{2+}-V_O^{2-} defect-pairs. Nevertheless, it is believed that the excess of V_O^{2-}, formed at higher sintering temperatures (1225°C and 1250°C), would be responsible for the creation of sub-band defect states and, consequently, an absorption increases in "all investigated" spectrum with increasing the sintering temperature. In more detail, by doping with Ni^{2+} the intrinsic bang gap is truly narrowed due to the more covalent nature of the Ni^{2+}-O bonding. The removal of oxygen ions from the O_6 octahedral cage during the sintering reduces the coordination number of the Ni^{2+} ions to five, also changing the bonding geometry from octahedral to a square pyramidal. In comparison with O_6 octahedral cage, such change lifts the degeneracy of the Ni^{2+} $3d_z^2$ and $3d_{x^2-y^2}$ orbitals. The $3d_{x^2-y^2}$ and $3d_z^2$ rise toward the top of valence band thus, also contributing to the intrinsic band gap narrowing.[35,45]

More importantly, by continuously increasing the sintering temperature, after the saturation of the formation of the Ni^{2+}-V_O^{2-} defect-pairs (that means one V_O^{2-} for each Ni^{2+} ion), the additional amount of V_O^{2-} introduces energy levels within the forbidden band (sub-band states), thus increasing the absorption at lowers energies. This absorption is reflected in the appearance of add-on shoulders in

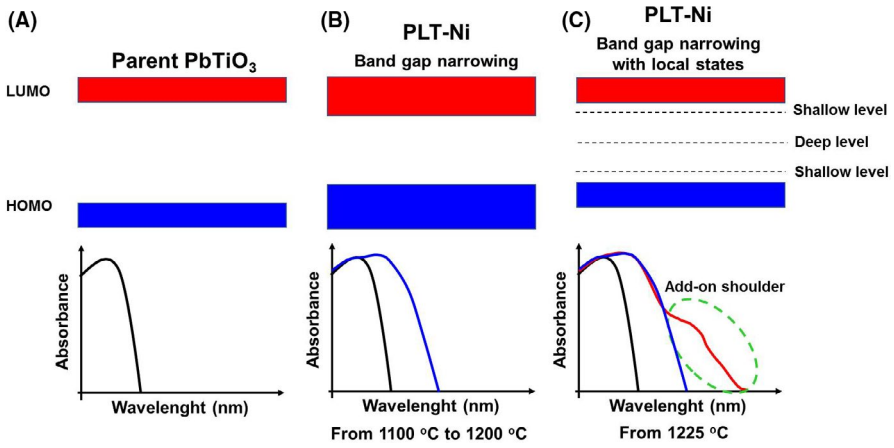

FIGURE 7 Tentative scheme for the electronic band structure of $(Pb_{0.8}La_{0.2})(Ti_{0.9}Ni_{0.1})O_3$ ceramics: (A) band structure and the optical absorption curve of the $PbTiO_3$; (B) red-shift of the absorption curve due to the band gap narrowing and; (C) absorption curve with an add-on shoulder due to the excess of V_O^{2-} extending the light absorption curve to longer wavelengths. Tentative schematic picture based on the Ref. [46] [Color figure can be viewed at wileyonlinelibrary.com]

the edge of the absorption curve for the samples sintered mainly at 1225°C and 1250°C.

In summary, it is believed that the changes in the optical absorption curve of the $(Pb_{0.8}La_{0.2})(Ti_{0.9}Ni_{0.1})O_3$ ceramics results from the intrinsic band gap narrowing, related to both Ni^{2+}-O and Ni^{2+}-V_O^{2-} bonding defects that are the dominant defects for the samples sintered at lower temperatures. For the samples sintered at higher temperatures, besides the intrinsic bag gap narrowing, sub-band states are also introduced due to the formation of additional and unavoidable V_O^{2-}. Adopting a schematic picture used by Liu and Wu,[46] Figure 7A,B are tentative schemes for the modification of the band structures of PLT-Ni. Figure 7A depicts a schematic band structure and the optical absorption curve of the parent $PbTiO_3$; in Figure 7B it is illustrated the red-shift of the absorption curve due to a true band gap narrowing due to the Ni^{2+}-V_O^{2-} defect-pairs and; finally, Figure 7C represents the absorption curve with an add-on shoulder due to the excess of V_O^{2-}, thus extending the light absorption curve to longer wavelengths.

Besides the optical properties, the focus of this work, it is also highlighted that the sintering temperature modified the character of the ferroelectric phase transition from diffuse to a sharper one, as observed in the dielectric and the thermal expansion measurements (Figures 3 and 4). We believe that these results also support our hypothesis about the formation of the extra amount of V_O^{2-} due to the sintering and the establishment of a spontaneous polarization below the phase transition temperature. Indeed, density functional theory predicts that V_O^{2-} associated with Ni^{2+} gives rise to significant distortions of the remaining O cage.6 This increases all cation displacements, leading to a higher polarization compared to the parent host, as verified in Figures 1B and 2. The increase in the *c*/*a* ratio may be associated with a more covalent bond of the Ni^{2+}-O and Ni^{2+}-V_O^{2-} defects, compared to the Ti-O bonds, increasing the displacive nature of the ferroelectric phase transition.

4 | CONCLUSION

In this work, it was shown that the bang gap energy of $(Pb_{0.8}La_{0.2})(Ti_{0.9}Ni_{0.1})O_3$ ceramics can be tailored by the sintering temperature. The band gap was reduced from approximately 2.67 to 1.99 eV by increasing the sintering temperature from 1100°C to 1250°C. It was inferred that the formation of V_O^{2-} and their ordering in the lattice during the sintering can explain such changes in the optical properties. By assuming this hypothesis, the optical properties, related to the band gap narrowing, can be associated with optical transitions due to the lift of the degeneracy of the Ni^{2+} $3d_z^2$ and $3d_{x^2-y^2}$ orbitals, and to a change of the O_6 octahedral cage, from octahedral to a square pyramid. Additional unavoidable V_O^{2-}, formed during the sintering process, were responsible for additional lower-energy absorbing states.

ACKNOWLEDGMENTS

The authors thank FAPESP (Proc. 2017/13769-1 and 2019/03110-8), CNPq, and FINEP for the financial support. The authors also thank the Federal University of São Paulo for providing the core research facilities—NAPCEM.

ORCID

Mahmoud S. Alkathy https://orcid.org/0000-0001-9704-3418
Manuel H. Lente https://orcid.org/0000-0002-7294-1411

REFERENCES

1. Grinberg ID, West V, Torres M, Gou G, Stein DM, Wu L, et al. Perovskite oxides for visible-light-absorbing ferroelectric and photovoltaic materials. Nature. 2013;503:509–12.
2. Zhou W, Deng H, Yang P, Chu J. Structural phase transition, narrow band gap, and room-temperature ferromagnetism in $[KNbO_3]_{1-x}[BaNi_{1/2}Nb_{1/2}O_{3-\delta}]_x$ ferroelectrics. Appl Phys Lett. 2014;105:111904.
3. Yang SY, Seidel J, Byrnes SJ, Shafer P, Yang C-H, Rossell MD, et al. Above-band gap voltages from ferroelectric photovoltaic devices. Nat Nanotechnol. 2010;5:143–7.
4. Zhang J, Su X, Shen M, Dai Z, Zhang L, He X, et al. Enlarging photovoltaic effect: a combination of classic photoelectric and ferroelectric photovoltaic effects. Sci Rep. 2013;3:2109.
5. Yang X, Su X, Shen M, Zheng F, Xin Y, Zhang L, et al. Enhancement of photocurrent in ferroelectric films via the incorporation of narrow band gap nanoparticles. Adv Mater. 2012;24:1202–8.
6. Bennett JW, Grinberg I, Rappe AM. New highly polar semiconductor ferroelectrics through d^8 Cation-O vacancy substitution into $PbTiO_3$: a theoretical study. J Am Chem Soc. 2008;130(51):17409–12.
7. Fridkin VM. Bulk photovoltaic effect in noncentrosymmetric crystals. Crystallogr Rep. 2001;46:654–8.Translated from Kristallografiya. 2001;46:722–6.
8. Gou GY, Bennett JW, Takenaka H, Rappe AM. Post density functional theoretical studies of highly polar semiconductive $Pb(Ti_{1-x}Ni_x)O_{3-x}$ solid solutions: Effects of cation arrangement on the band gap. Phys Rev B. 2011;83:205115.
9. Choi WS, Chisholm MF, Singh DJ, Choi T, Jellison GE Jr, Lee HN. Wide band gap tunability in complex transition metal oxides by site-specific substitution. Nat Commun. 2012;3:689.
10. Arima T, Tokura Y, Torrance JB. Variation of optical gaps in perovskite-type 3*d* transition-metal oxides. Phys Rev B. 1993;48:17006–9.
11. Shirane G, Pepinsky R. X-ray and neutron diffraction study of ferroelectric $PbTiO_2$. Acta Cryst. 1956;9:131–40.
12. Qi T, Curnan MT, Kim S, Bennett JW, Grinberg I, Rappe AM. First-principles study of band gap engineering via oxygen vacancy doping in perovskite $ABBO_3$ solid solutions. Phys Rev B. 2011;84:245206.
13. Jaiswar S, Mandal KD. Evidence of enhanced oxygen vacancy defects inducing ferromagnetism in multiferroic $CaMn_7O_{12}$ manganite with sintering time. J Phys Chem C. 2017;121:19586–601.
14. Singh G, Tiwari VS, Gupta PK. Role of oxygen vacancies on relaxation and conduction behaviour of $KNbO_3$ ceramic. J Appl Phys. 2010;107:064103.
15. Zhang Z, Wu P, Lu L, Shu C. Ab initio study of formations of neutral vacancies in ferroelectric $PbTiO_3$ at different oxygen atmospheres. J Alloys Comp. 2008;449:362–5.
16. Pan X, Yang M-Q, Fu X, Zhang N, Xu Y-J. Defective TiO_2 with oxygen vacancies: synthesis, properties and photocatalytic applications. Nanoscale. 2013;5:3601–14.
17. Yang Y, Wang Y, Yin S. Oxygen vacancies confined in SnO_2 nanoparticles for desirable electronic structure and enhanced visible-light photocatalytic activity. Appl Surface Sci. 2017;420:399–406.
18. Li M, Hebenstreit W, Diebold U, Tyryshkin AM, Bowman MK, Dunham GG, et al. The influence of the bulk reduction state on the surface structure and morphology of rutile TiO_2 (110) single crystals. J Phys Chem B. 2000;104:4944–50.
19. Urbach F. The long-wavelength edge of photographic sensitivity and the electronic absorption of solids. Phys Rev. 1953;92:1324.
20. Akshay VR, Arun B, Mandal G, Vasundhara M. Visible range optical absorption, Urbach energy estimation and paramagnetic response in Cr-doped TiO_2 nanocrystals derived by a sol-gel method. Phys Chem Chem Phys. 2019;21:12991–3004.
21. Choudhury B, Choudhury A. Oxygen defect dependent variation of band gap, Urbach energy and luminescence property of anatase, anatase–rutile mixed-phase and of rutile phases of TiO_2 nanoparticles. Physica E. 2014;56:364–71.
22. Li J, Chu D. Chapter 4: energy band engineering of metal oxide for enhanced visible light absorption. In: Lin Z, Ye M, Wang M, editors. Multifunctional photocatalytic materials for energy. Amsterdam, The Netherlands: Elsevier; 2018. p. 49–78.
23. Yao L, Inkinen S, van Dijken S. Direct observation of oxygen vacancy-driven structural and resistive phase transitions in $La_{2/3}Sr_{1/3}MnO_3$. Nat Commun. 2017;8:14544.
24. Lv Y, Yao W, Ma X, Pan C, Zong R, Zhu Y. The surface oxygen vacancy induced visible activity and enhanced UV activity of a ZnO_{1-x} photocatalyst. Catal Sci Technol. 2013;3:3136–46.
25. Persson K.Materials data on TiPbO3 (SG: 99) by materials project. 2014. https://doi.org/10.17188/1195590.
26. He Z, Ma J. Constitutive modelling of the densification of PZT ceramics. J Phys Chem Sol. 2003;64:117–83.
27. Kim T-Y, Jang HM, Cho SM. Effects of La doping on the cubic–tetragonal phase transition and short-range ordering in $PbTiO_3$. J Appl Phys. 2002;91:336–42.
28. Neves PP, Doriguetto AC, Mastelaro VR, Lopes LP, Mascarenhas YP, Michalowicz A, et al. XAS and XRD structural characterization of lanthanum-modified $PbTiO_3$ ceramic materials. J Phys Chem B. 2004;108:14840–9.
29. Lee S, Rossetti GA Jr, Liu Z-K, Randall CA. Intrinsic ferroelectric properties of the nonstoichiometric perovskite oxide $Ba_{1-x}Ti_{1-y}O_{3-x-2y}$. J Appl Phys. 2009;105:093519.
30. Scott JF, Gardner J. Ferroelectrics, multiferroics and artefacts: Lozenge-shaped hysteresis and things that go bump in the night. Mater Today. 2018;21:553–62.
31. Unruan M, Prasatkhetragarn A, Laosiritaworn Y, Ananta S, Ngamjarurojana A, Yimnirun R, et al. Measurement of thermal strain and total polarization estimation of lead zirconate titanate–lead zinc niobate ceramics. J Mater Sci. 2012;47:5801–5.
32. Jiménez R, Jiménez B, Carreaud J, Kiat JM, Dkhil B, Holc J, et al. Transition between the ferroelectric and relaxor states in $0.8(PbMg_{1/3}Nb_{2/3})O_3$–$0.2PbTiO_3$ ceramics. Phys Rev B. 2006;74:184106.
33. Viezbicke BD, Patel S, Davis BE, Birnie DP III. Evaluation of the Tauc method for optical absorption edge determination: ZnO thin films as a model system. Phys Status Solidi B. 2015;252:1700–10.
34. Gennari RC, Lang R, Eiras JA, Lente MH. Effects of sintering process on the structural, dielectric and optical absorption properties of $KNbO_3$-based ceramics. J Am Ceram Soc. 2018;102:3923.
35. Zhou W, Deng H, Yu L, Yang P, Chu J. Optical band-gap narrowing in perovskite ferroelectric ABO_3 ceramics (A=Pb, Ba; B=Ti) by ion substitution technique. Ceram Int. 2015;41:13389–92.
36. Zhou W, Deng H, Yu L, Yang P, Chu J. Magnetism switching and band gap narrowing in Ni-doped $PbTiO_3$ thin films. J Appl Phys. 2015;117:194102.

37. Baiju KG. Hydrothermal synthesis, dielectric properties of barium titanate, cobalt doped barium titanate, and their graphene nanoplatelet composites. Asia-Pac J Chem Eng. 2020;15:e2550.
38. Dhar A, Mansingh A. Optical properties of reduced lithium niobate single crystals. J Appl Phys. 1990;68:5804.
39. Chermette H, Pertosa P, Michel-Calendini FM. Molecular orbital study of satellites in XPS spectra of $BaTiO_3$ and TiO_2. Chem Phys Lett. 1980;69:240–5.
40. Suriyaprakash J, Xu YB, Zhu YL, Yang LX, Tang YL, Wang YJ, et al. Designing of metallic nanocrystals embedded in non-stoichiometric perovskite nanomaterial and its surface-electronic characteristics. Sci Rep. 2017;7:8343.
41. Moulder JF, Stickle WF, Sobol PE, Bomben KD. Handbook of X-ray photoelectron spectroscopy. Eden Prairie, MN: Perkin-Elmber Corporation; 1992.
42. López JM, Gilbank AL, García T, Solsona B, Agouram S, Torrente-Murciano L. The prevalence of surface oxygen vacancies over the mobility of bulk oxygen in nanostructured ceria for the total toluene oxidation. Appl Catal B. 2015;174–175:403–12.
43. Chang F-M, Brahma S, Huang J-H, Wu Z-Z, Lo K-Y. A strong correlation between optical properties and mechanism in deficiency of normalized self-assembly ZnO nanorods. The strong correlation between optical properties and mechanism in deficiency of normalized self-assembly ZnO nanorods. Sci Rep. 2019;9:905.
44. Prakash A, Bahadur D. Chemically derived defects in zinc oxide nanocrystals and their enhanced photo-electrocatalytic activities. Phys Chem Chem Phys. 2014;16:21429–37.
45. Qi T, Grinberg I, Rappe AM. Band-gap engineering via local environment in complex oxides. Phys Rev B. 2011;83:224108.
46. Li J, Wu N. semiconductor-based photocatalysts and photoelectrochemical cells for solar fuel generation: a review. Catal Sci Technol. 2015;5:1360–84.

SUPPORTING INFORMATION

Additional supporting information may be found online in the Supporting Information section.

How to cite this article: Vargas NF, Alkathy MS, Eiras JA, Mastelaro VR, Lente MH. Sintering-driven effects on the band gap of $(Pb,La)(Ti,Ni)O_3$ photovoltaic ceramics. *J Am Ceram Soc*. 2021;104:2600–2609. https://doi.org/10.1111/jace.17682